frontiers | Frontiers in Marine Science

TYPE Original Research
PUBLISHED 04 January 2024
DOI 10.3389/fmars.2023.1296836

OPEN ACCESS

EDITED BY
Wonho Yih,
Kunsan National University, Republic of Korea

REVIEWED BY
Kwang-Sik Albert Choi,
Jeju National University, Republic of Korea
Sebastian G. Gornik,
Heidelberg University, Germany

*CORRESPONDENCE
Sunju Kim
sunkim@pknu.ac.kr

†Retired

RECEIVED 19 September 2023
ACCEPTED 05 December 2023
PUBLISHED 04 January 2024

CITATION
Yoo J, Kim S and Coats DW (2024) Morphology of *Hobagella saltata* n. gen. and n. sp. (Syndiniophyceae, Miozoa) infecting the marine dinoflagellate *Cucumeridinium coeruleum* (Dinophyceae, Miozoa) and its potential onshore advection.
Front. Mar. Sci. 10:1296836.
doi: 10.3389/fmars.2023.1296836

Morphology of *Hobagella saltata* n. gen. and n. sp. (Syndiniophyceae, Miozoa) infecting the marine dinoflagellate *Cucumeridinium coeruleum* (Dinophyceae, Miozoa) and its potential onshore advection

Jiae Yoo[1], Sunju Kim[1*] and D. Wayne Coats[2†]

[1]Major of Oceanography, Division of Earth Environmental System Science, Pukyong National University, Busan, Republic of Korea, [2]Smithsonian Environmental Research Center, Edgewater, MD, United States

Over the past decade, molecular phylogenies have placed endoparasites of the genus *Eduboscquella* in a distinct subclade within clade 4 of the Marine Alveolate (MALV) Group I. Recently, however, rRNA gene sequences have become available for four novel *Eduboscquella*-like species that infect dinoflagellates, with phylogenies including these sequences indicating that the genus *Eduboscquella* is paraphyletic. Here, we provide a morphological characterization of the intracellular and extracellular life-cycle stages of a novel species that infects *Cucumeridinium coeruleum*, a warm water pelagic species sometimes found in coastal environments. We formally describe the novel parasite, *Hobagella saltata* n. gen, n. sp., and identify a constellation of morphological and developmental characters that distinguish it, as well as *Eduboscquella melo* and *E. nucleocola*, both parasites of dinoflagellates, from *Eduboscquella* species that infect ciliates. We recommend the reassignment of *E. melo* and *E. nucleocola* as *Hobagella melo* n. comb. and *H. nucleocola* n. comb., respectively. We also propose the family Hobagellidae for these three congeners. We anticipate that the character set developed for distinguishing species of *Eduboscquella* and *Hobagella* will be valuable for sorting other *Eduboscquella*-*Hobagella*-like taxa scattered across the Group I phylogeny and will provide insight into morphological evolutionary patterns within Group I. Lastly, we consider the potential influence of summer-fall typhoons on the occurrence of *H. saltata* and its host *C. coeruleum* in near-shore waters along the southeastern coast of Korea and propose a hypothesis regarding the northward transport and

onshore advection of host and parasite populations. If future research supports the hypothesized mechanisms, it could help us better understand parasite distribution and potential changes in biogeography associated with ongoing global changes in surface seawater temperature.

KEYWORDS

Cucumeridinium, dinoflagellate, endoparasite, *Euduboscquella*, life cycle, morphology, syndiniophycean, typhoon

1 Introduction

In their revision of the dinoflagellate genus *Duboscquella* Chatton, 1920, Coats et al. (2012) considered the type species *D. tintinnicola* Lohmann, 1908 to be an extracellular parasite of tintinnids, with morphological features consistent with those of core dinoflagellates. The authors recommended the transfer of *D. tintinnicola* to the subphylum Dinokaryota Fensome et al., 1993 as the sole representative of a monotypic genus but retained intracellular parasites previously classified as species of *Duboscquella* within the subphylum Syndinea Corliss, 1984, creating a new genus, *Euduboscquella*, and a family, Euduboscquellidae. Thus far, 10 species of *Euduboscquella* have been described as intranuclear or intracytoplasmic parasites of their ciliate and dinoflagellate hosts: seven species from tintinnids, one from aloricate ciliates, and two from heterotrophic dinoflagellates.

Euduboscquella species have a cuticularized episomal surface, often referred to as the shield, bordered by a fibrous annulus (= perinema or perinematic ring), that appears flat to slightly domed during early to mid-infection. In ciliate hosts, the shield of the mature trophont covers about half of the parasite surface (Coats and Moon, 2022; Yoo et al., 2022). It is creased by one or more grooves that are either intertwined in a brain-like fashion, radiate centripetally from the center of the shield, or course linearly across the episome (Choi et al., 2021). The shields of the two species known to infect dinoflagellates have centripetal grooves during early development, which are subsequently arranged as meridians as the episome expands, covering almost the entire surface of the mature trophont (Cachon, 1964).

Several fibrous elements, known to be microtubular in *E. cachoni* (Coats and Moon, 2022), originate from the perinema of *Euduboscquella* species, course beneath the episome, and in some instances appear to support the grooves of the shield. In *Euduboscquella* species that infect ciliates, some of the fibers emanating from the perinema form a funnel-shaped, non-functional cytopharynx known as the "lamina pharyngae" (Cachon, 1964). The two species infecting dinoflagellates, however, lack a "lamina pharyngae", having instead bundles of microtubules directed toward and becoming associated with the parasite nucleus.

At maturity, *Euduboscquella* species infecting tintinnids undergo a complicated morphogenetic process that does not rupture the host pellicle, enabling ingestion of all or part of the host cell during parasite egress (Cachon, 1964; Coats and Moon, 2022). The tomont, an extracellular pre-division stage, is produced by species infecting tintinnids and has a conspicuous food vacuole that undergoes digestion before and during sporogenesis. In contrast, *E. melo*, a parasite of *Noctiluca scintillans* (considered *N. miliaris* by Cachon), reaches maturity and undergoes sporogenesis inside the theca of its moribund host, whereas *E. nucleocola*, a parasite of *Leptodiscus medusoides*, elongates at maturity to rupture its host pellicle, with sporogenesis occurring in the surrounding water. Neither of the parasites infecting dinoflagellates incorporate host material into a conspicuous food vacuole (Cachon, 1964); however, Cachon thought that foreign particles rarely observed in *E. melo* might represent host material accidentally taken up before sporogenesis. Thus, *Euduboscquella* species infecting ciliates differ from those infecting dinoflagellates in at least four significant ways: shield pattern in the mature trophont, presence of a "lamina pharyngae," process of parasite egress, and occurrence of a conspicuous food vacuole in the tomont.

SSU rRNA gene phylogenies have shown that the genus *Euduboscquella* forms its own specific subclade within clade 4 of the Marine Alveolate (MALV) Group I (Bachvaroff et al., 2012; Choi et al., 2021). However, the SSU rRNA sequences available for such phylogenetic analyses are restricted to *Euduboscquella* species that infect tintinnids, leaving in question the phylogenetic position of *Euduboscquella* species that infect aloricate ciliates and dinoflagellates. Yoo et al. (2022) recently examined four morphologically distinct *Euduboscquella*-like parasites, each infecting a different heterotrophic dinoflagellate species. Phylogenetic analyses indicated that parasites morphologically identifiable as *Euduboscquella* species were paraphyletic, thus indicating a need to revise the genus *Euduboscquella*. More recently, Holt et al. (2023) provided molecular sequences of unidentified Ichthyodinida species infecting dinoflagellates that we include in an updated MALV Group I phylogeny. Here, we provide a formal description of a *Euduboscquella*-like parasite that infects *Cucumeridinium coeruleum* in South Korean coastal waters, referred to as *Euduboscquella* sp. ex *C. coeruleum* (OP445718-21) by

Yoo et al. (2022). We also compared the morphology of the parasite infecting *C. coeruleum* with that of the species currently assigned to the genus *Eudubosquella*, erect *Hobagella* n. gen., and populated the new genus with our novel parasite, *H. saltata* n. sp., *H. melo* n. comb., and *H. nucleocola* n. comb. Finally, we discuss the potential influence of tropical storms on the presence of *H. saltata* along the southeastern coast of Korea.

2 Materials and methods

2.1 Sample collection

Samples containing *Cucumeridinium coeruleum* were collected from Yongho Harbor, Busan, ROK (35°08′00″N, 129°06′55″E) on 26–28 August 2019 and from Youngdo Harbor, Busan, ROK (35° 04′42″N, 129°04′53″E) on 10 September 2022. Surface water temperature and salinity were measured *in situ* using a YSI Pro30 Conductivity, Salinity Instrument (YSI Inc., Yellow Springs, US). Samples of surface water collected using a bucket and net-tow material obtained by vertically towing a 20-µm mesh plankton net through the upper 2 m of the water column were distributed to 50 mL PE bottles. Subsamples of net collections were fixed immediately with neutral Lugol's solution (final concentration of 0.04% iodine [w/v]; 0.06% potassium iodide [w/v]) or glutaraldehyde (final concentration of 1%). Fixed and unfixed samples were transported to the lab within 30 min, with the former stored in the dark at 4°C and the latter maintained at near ambient water temperature (20–23°C).

2.2 Parasite morphology, development, and cytology

To detect *C. coeruleum* infected by *H. saltata*, plankton samples were examined using a Leica DM IL LED inverted microscope (Leica Microsystems, Wetzlar, Germany) or a Zeiss Invert microscope (Carl Zeiss Inc., Oberkochen, Germany). Infected *C. coeruleum* were individually isolated using a Pasteur pipette (Hilgenberg, Münnerstadt, Germany) and washed at least three times in surface water passed through a 0.2-µm cellulose acetate syringe filter (Toyo roshi kaisha ltd., Tokyo, Japan). Isolated specimens were transferred to 24-well plates (SPL Life Sciences, Gyeonggi-do, South Korea) containing filtered surface water and incubated at room temperature (20–23°C). To document parasite development, the specimens were monitored over time, photographed, and video-recorded using a full HD MediCAM-K/2 (Comart System Co., Ltd., Seoul, Korea) coupled with a Zeiss Invert microscope. For more detailed morphological observations, the specimens were transferred to microscope slides, examined, and photographed at ×400 to ×1000 magnifications using a Zeiss Axio Imager2 equipped with AxioCam HRc (Carl Zeiss Inc.) interfaced with a PC running Zen software (Carl Zeiss Inc.), and then returned to 24-well plates.

To determine parasite cytology and prevalence, *C. coeruleum* cells were randomly isolated from net sample collected on 27 August 2019, fixed with modified Bouin's fluid (Coats and Heinbokel, 1982; final concentration of 5%, w/v), and stored at room temperature. *C. coeruleum* cells were similarly isolated from glutaraldehyde and Lugol's iodine-fixed net samples collected on 26–28 August 2019. Isolated preserved cells were processed by quantitative protargol staining (Montagnes and Lynn, 1993), and all infected host cells were photographed for morphological measurements. Morphological measurements were obtained using AxioVision SE64 Rel 4.9.1 software (Carl Zeiss Inc.), with mean ± standard error (SE) of the mean and sample size (n) reported in the text and tables. Parasite prevalence (percentage of infected host cells) was determined by scoring all specimens present on the stained slides as either infected or uninfected.

Graphics and statistical comparisons of host and parasite morphometrics were performed using SigmaPlot v13 (Systat Software Inc., San Jose, CA, USA). The International Code of Zoology Nomenclature was adopted for naming new taxa.

2.3 Sequence alignment and phylogenetic analyses

284 SSU rRNA gene sequences, including 14 sequences of *Eudubosquella* species that infect tintinnids, four sequences of *Hobalgella saltata* n. gen. n. sp., four of *Eudubosquella* species that infect dinoflagellates, four of *Ichthyodinium* species, and three sequences of unidentified Ichthyodinida species and 265 environmental sequences were retrieved from GenBank (http://www.ncbi.nlm.nih.gov) of NCBI (National Center for Biotechnology Information) to analyze MALV Group I phylogeny. The sequences were aligned using MAFFT version 7 (Katoh et al., 2019). The aligned dataset was adjusted and the ambiguous regions at each end of the sequences were trimmed using MEGA-X (Kumar et al., 2018) and 1763 bp positions were applied for phylogenetic analyses. Maximum likelihood (ML) analysis was performed using a RAxML with the GTRGAMMA model and 2000 replicates with the rapid bootstrapping option.

3 Results

3.1 Environmental conditions and parasite prevalence

Hobagella saltata n. gen., n. sp. was observed in coastal waters near Busan, ROK, on four sampling dates: from Yongho Harbor on 26–28 August 2019 and from Youngdo Harbor on 10 September 2022 (Figure 1; Table 1). *C. coeruleum* was also present in samples collected from Yongho Harbor on the following dates: 23 August 2019, 22 September 2020, 18 and 30 September 2022, 9 and 15 October 2022, *H. saltata* was not observed on these dates. In both years, samples containing *H. saltata* were encountered after a tropical storm (Typhoon KROSA in 2019 and Typhoon HINNAMNOR in 2022) moved from south to north into the East Sea (Sea of Japan), either passing west or crossing over Japan. *Cucumeridinium coeruleum* infected by *H. saltata* occurred 10–12 d after the storm in 2019 and 4 d after the storm in 2022 (Figure 2).

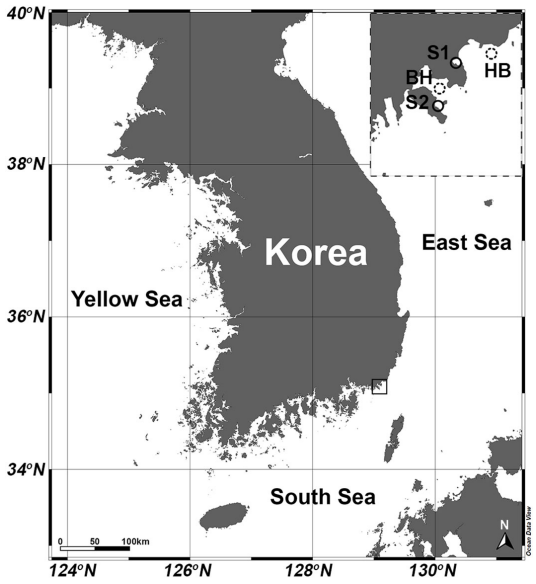

FIGURE 1
Map of study area showing locations of stations where *H. saltata* occurred (S1, Yongho Harbor; S2 Youngdo Harbor) and station locations for open-source data obtained by the Korea Hydrographic and Oceanographic Agency (KHOA): (http://www.khoa.go.kr/oceangrid/gis/category/reference/distribution.do). Downloaded data are presented for the Haeundae Beach Station (HB) from 1 August 2019 to 1 September 2019 and for the Busan Harbor Station (BH) from 20 August 2022 to 9 September 2022.

Net samples collected in 2019 revealed a diverse phytoplankton community with a diatom-dominated composition, whereas net phytoplankton collected in 2022 were extremely dense and almost entirely composed of diatoms. Water temperature for samples containing *H. saltata* was 1–2°C lower than sea surface temperature as the typhoons approached the Korean coast (cf. Table 1; Figure 2).

Host cells infected by *H. saltata* of sufficient size to be detected using an inverted or stereo microscope were uncommon in all samples, resulting in the isolation of only 10 specimens (eight in 2019 and two in 2022) for the examination of parasite morphology and development. Protargol-stained preparations of *C. coeruleum* arbitrarily isolated from *in vivo* and preserved net samples revealed that the prevalence of *H. saltata* ranged from 2–6% for dates in 2019 (Table 1). The number of hosts in the 2022 net samples was too low to permit assessment of parasite prevalence.

3.2 Morphology of uninfected *Cucumeridinium coeruleum*

Uninfected *C. coeruleum* had an ellipsoidal shape *in vivo*, with well-marked, equidistant longitudinal ridges and striking blue or, more rarely, purple pigmentation (Figure 3A). Uninfected host cells averaged 105.2 ± 3.2 by 54.1 ± 3.3 µm (n = 11) *in vivo* and contained a nucleus measuring 31.6 ± 3.5 by 25.0 ± 2.1 µm (n = 7 and 6, respectively) (Figure 3A; Table 2). After protargol impregnation, uninfected hosts averaged 104.4 ± 1.8 by 62.3 ± 1.4 µm n = 73), had a kidney-shaped nucleus that measured 22.3 ± 0.5 by 15.6 ± 0.3 µm (n = 73), contained multiple nucleoli, and had a slightly swollen nuclear envelope (Figures 3B, 4A).

3.3 Morphology and development of *H. saltata* n. gen., n. sp.

3.3.1 Early infections

Very early stages of the intracellular infection cycle of *H. saltata* were easily detected inside the host nucleus following protargol impregnation (Figures 3C, E, 4B). The smallest (presumably the earliest) such parasite was roughly spherical, measuring 13 by 12 µm. It had a large nucleus (8 µm in diameter) relative to its cell size, a single large nucleolus (5 by 4 µm), and a swollen host nuclear envelope (Figure 3C). Infection stages before entry into the host nucleus were at undetectable levels.

Very early stages of infection were difficult to detect *in vivo* (Figures 3D, 4C), and only two such parasites were isolated, one of which was examined during incubation. When isolated, the two specimens appeared as a clear, irregularly ovoid mass inside the host nucleus, measured 49–52 by 32–34 µm, and had a large spherical nucleus (24–25 µm in diameter) and nucleolus (14–15 µm diameter) (Figure 3D). After incubation for 5.5 h, the parasite showed a slight increase in size to 32 by 42 µm and had developed a clearly defined episomal shield creased by 15–20 short, centripetally arranged ribs, marking the transition into what we define as a mid-infection (Figure 3F).

TABLE 1 Sampling data and parasite prevalence for *Hobagella saltata* n. gen., n. sp. infecting *Cucumeridinium coeruleum*.

Site	Coordinates	Sampling date	Temp. (°C)	Sal.	Parasite prevalence (%)
Yongho Harbor, Busan, Korea	35°08′00″N, 129°06′55″E	August 26, 2019	25.7	32.8	5.1 (n = 227)
Yongho Harbor, Busan, Korea	35°08′00″N, 129°06′55″E	August 27, 2019	ND	ND	6.3 (n = 32)
Yongho Harbor, Busan, Korea	35°08′00″N, 129°06′55″E	August 28, 2019	25.0	32.3	2.5 (n = 77)
Youngdo Harbor, Busan, Korea	35°04′42″N, 129°04′53″E	Sept 10, 2022	24.2	29.8	ND

ND, no data.

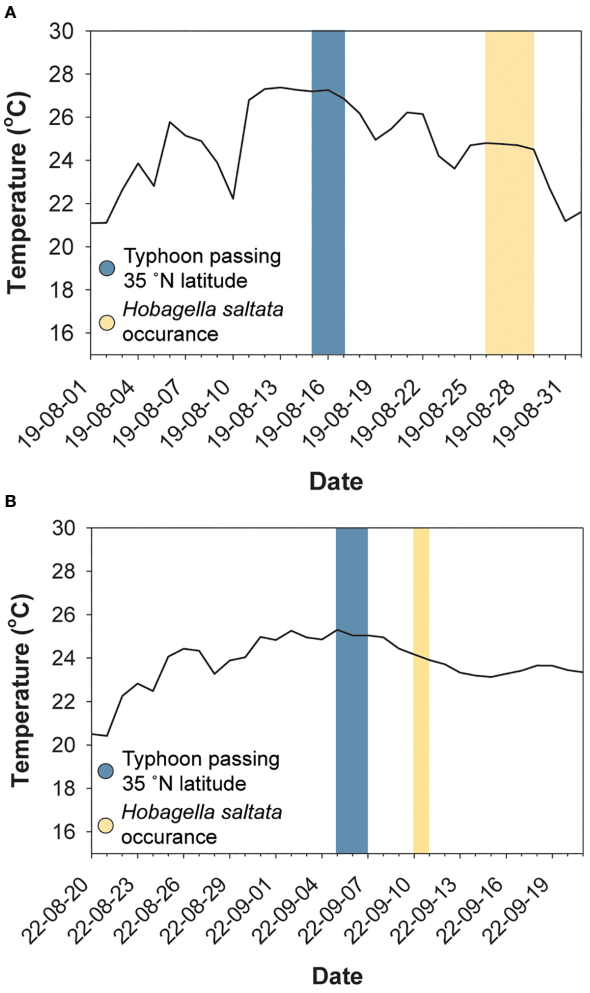

FIGURE 2
Surface water temperature (solid line) near Busan, ROK, dates when typhoons crossed latitudes corresponding to the southeast coast of Korea (blue shading), and dates when *Hobagella saltata* infected *Cucumeridinium coeruleum* (yellow shading). **(A)** Data for 2019, with water temperature for the Haeundae Beach Station. **(B)** Data for 2022, with water temperature for the Busan Harbor station. Selected station data were the nearest available to Yongho Harbor in 2019 and to Youngdo Harbor in 2022.

Collectively, *in vivo* and cytological observations for early infections indicate that an increase in parasite size, once inside the host nucleus, is accompanied by an increase in nuclear and nucleolar size, as well as a change in the form of the host nucleus from kidney bean-shaped to spherical, with the host's partially digested nucleoplasm distributed peripherally and its nuclear envelope becoming noticeably swollen in cytological preparations (Figures 3C–E, 5).

3.3.2 Mid- to late-infections

When isolated, all other *H. saltata* examined *in vivo* were in the mid- to late-stages of the intracellular infection cycle (defined as ≤half and > half of the parasite surface covered by the episomal shield, respectively) and were visible as a large, clear to yellowish mass occupying much of the host cytoplasm (Figures 3G, H, J, K, 4D–F). These cells had a shape similar to a prolate spheroid, but demonstrated slight anterior-posterior flattening, averaging 74.2 ± 4.6 µm (n = 15) in maximum cell dimension, 54.9 ± 5.2 µm (n = 12) in a minimum cell dimension, and 61.3 ± 4.4 µm (n = 6) in anterior-posterior dimension (= cell length) (Table 3). Their single, spherical to ovoid nucleus and nucleolus (Figures 3G, K, 4D–F) measured 29.5 ± 1.3 by 27.6 ± 1.6 µm (n = 11) and 16.5 ± 0.8 by 15.1 ± 0.9 µm (n = 8), respectively (Table 3). The ovoid episome of mid- to late-stage *H. saltata* had a dome-shaped appearance, covered 1/4 to 3/4 of the parasite's surface, and measured 68.7 ± 5.7 µm (n = 8) in maximum dimension, 57.9 ± 6.0 µm (n = 4) in minimum dimension, and 35.4 ± 9.7 µm (n = 7) in anterior-posterior dimension. Distinct episomal ribs, 35.9 ± 1.7 (n = 8) in number, radiated outward from the center of the shield and coursed posteriad over the domed episomal surface. In addition, fibrous bundles originating from the episome extended into the parasite hyposome and were adjacent to the nucleus (Figure 3H inset). Very few mid- to late-infections were present in protargol preparations, but showed features similar to those seen *in vivo*, except for a highly swollen host nuclear envelope (Figure 3I) not seen *in vivo*. Host cells infected by mid- to late-stages of *H. saltata* appeared swollen due to the parasite, measuring 137.2 ± 5.1 (n = 9) by 78.8 ± 5.9 µm (n = 8) *in vivo* (Table 3), with cell width being significantly greater than that of uninfected host cells (t-test: $p < 0.001$).

The episomes of freshly isolated mid- to late-stage infections gradually expanded over time, with a concurrent decrease in hyposome surface area. Consequently, the centripetal grooves became bipolar. One of the bipolar grooves, the ventral furrow, had a slightly greater width and depth. Flagella were not observed. As the parasite approached maturity, the cell began to elongate and the episome expanded more rapidly. For example, the episome of the most advanced parasite isolated measured 82 µm in maximum dimension, 75 µm in minimum dimension, and 55 µm in anterior-posterior dimension, with 34 centripetal grooves (Figures 3J, K, 4E, F). At that time, the parasite cell had the same maximum and minimum dimensions as the episome, but an anterior-posterior dimension of 62 µm, Thus, the shield covered approximately 80% of the parasite cell surface. During the following 1 h and 40 min, the specimen became more spherical, with the maximum dimension of the parasite cell and episome being 84 µm and the anterior-posterior dimension of the cell and episome being 70 µm and 62 µm, respectively; the shield covered approximately 90% of the parasite's surface (Figure 3L). The specimen then quickly elongated over the next 5 min, taking on a pointed, acorn-shaped profile, with the parasite cell and episome measuring 76 µm in maximum dimension and the anterior-posterior dimension of the parasite cell and episome being 76 µm and 69 µm, respectively; the shield covered approximately 95% of the parasite's surface (Figures 3M, 4G). The mature, pre-emergent parasite appeared tightly packed inside the host pellicle and had a single large nucleus without an apparent nucleolus.

3.3.3 Parasite emergence

The egress of *H. saltata* began with the rupture of the dorsal surface of the host, where it contacted the pointed apex of the parasite (Figures 4H, 6A). Emergence took approximately 3 min to complete. During this time, the parasite shed the host's pellicle and

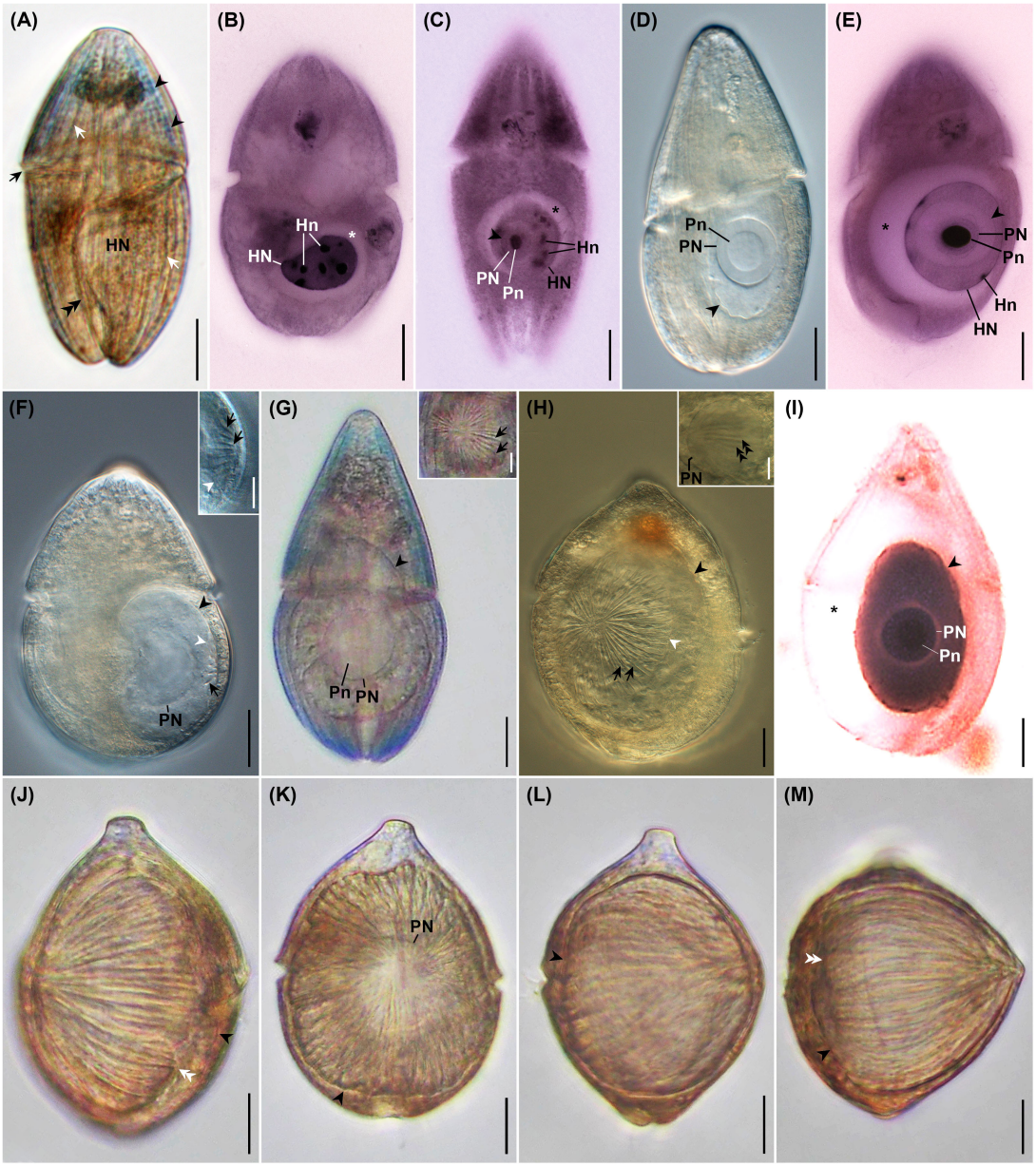

FIGURE 3
Photomicrographs of uninfected *Cucumeridinium coeruleum in vivo* **(A)** and after protargol impregnation **(B)**, and *Hobagella saltata* n. gen., n. sp. infecting *C. coeruleum in vivo* **(D, F–H, J–M)** and after protargol impregnation **(C, E, I)**. **(A)** Uninfected *C. coeruleum* with blue pigmentation (black arrowheads), longitudinal equidistant ridges (white arrows), and nucleus (HN). The black arrow and double black arrowhead indicate the girdle and sulcus, respectively. **(B)** Protargol impregnated uninfected *C. coeruleum* showing a nucleus (HN) with several nucleoli (Hn). Star marks space due to swollen, host nuclear envelope. **(C)** Protargol-impregnated parasite in very early infection showing nucleus (PN) and conspicuous nucleolus (Pn) within host nucleus (HN). Black arrowhead and star mark the margin of the parasite and swelling of the host nuclear envelope, respectively. **(D)** Early parasite trophont showing nucleus (PN) with large nucleolus (Pn) *in vivo*. **(E)** Early infection after protargol impregnation showing parasite nucleus (PN) with densely staining nucleolus (Pn). Growth of the parasite pushes host nucleoli (Hn) to the margin of the host nucleus (HN). Star marks swelling of host nuclear envelope. **(F)** Same specimen as **(D)** after 5h 30 min. Several short grooves (black arrow) crease the parasite episome. Black and white arrowheads indicate the margin of the parasite and episome, respectively. Inset: high magnification of episome and episomal grooves (black arrows); white arrowhead indicates margin of episome. **(G)** Mid-infection with parasite nucleus (PN) and nucleolus (Pn) visible. Inset: anterior view of episome at higher magnification revealing centripetal grooves and ridges (black arrows). **(H)** Mid-stage parasite trophont with conspicuous centripetal grooves and ridges (black arrows) on episome. Black and white arrowheads mark the margin of the parasite and parasite episome, respectively. Inset: focal plane near the surface of parasite nucleus (PN) showing association with episomally derived fibers (double black arrowheads). **(I)** A protargol-impregnated parasite following consumption of host nucleoplasm and nucleoli. Black arrowhead and star respectively mark the margin of the parasite and the space formed by the very swollen host nuclear envelope; PN, parasite nucleus; Pn, parasite nucleolus. **(J)** A nearly mature trophont in lateral view with grooves extending from cell apex to the margin of episome (white double arrowheads). The black arrowhead indicates the margin of the hyposome. **(K)** Same specimen as **(J)** in the anterior view. The arrowhead indicates the margin of the parasite. Parasite nucleus (PN), **(L)** Same specimen as **(J)** after 1 h 40 min. showing moderate anterior-posterior elongation of the parasite. The arrowhead indicates the parasite margin. **(M)** Same specimen as **(L)** after 5 min. showing more extensive elongation of the cell and formation of an acute apex. Black arrowhead and white double arrowheads indicate the margin of the hyposome and episome, respectively. Scales bar = 20 µm except for inserts. Scale bars for insets = 10 µm.

10.3389/fmars.2023.1296836

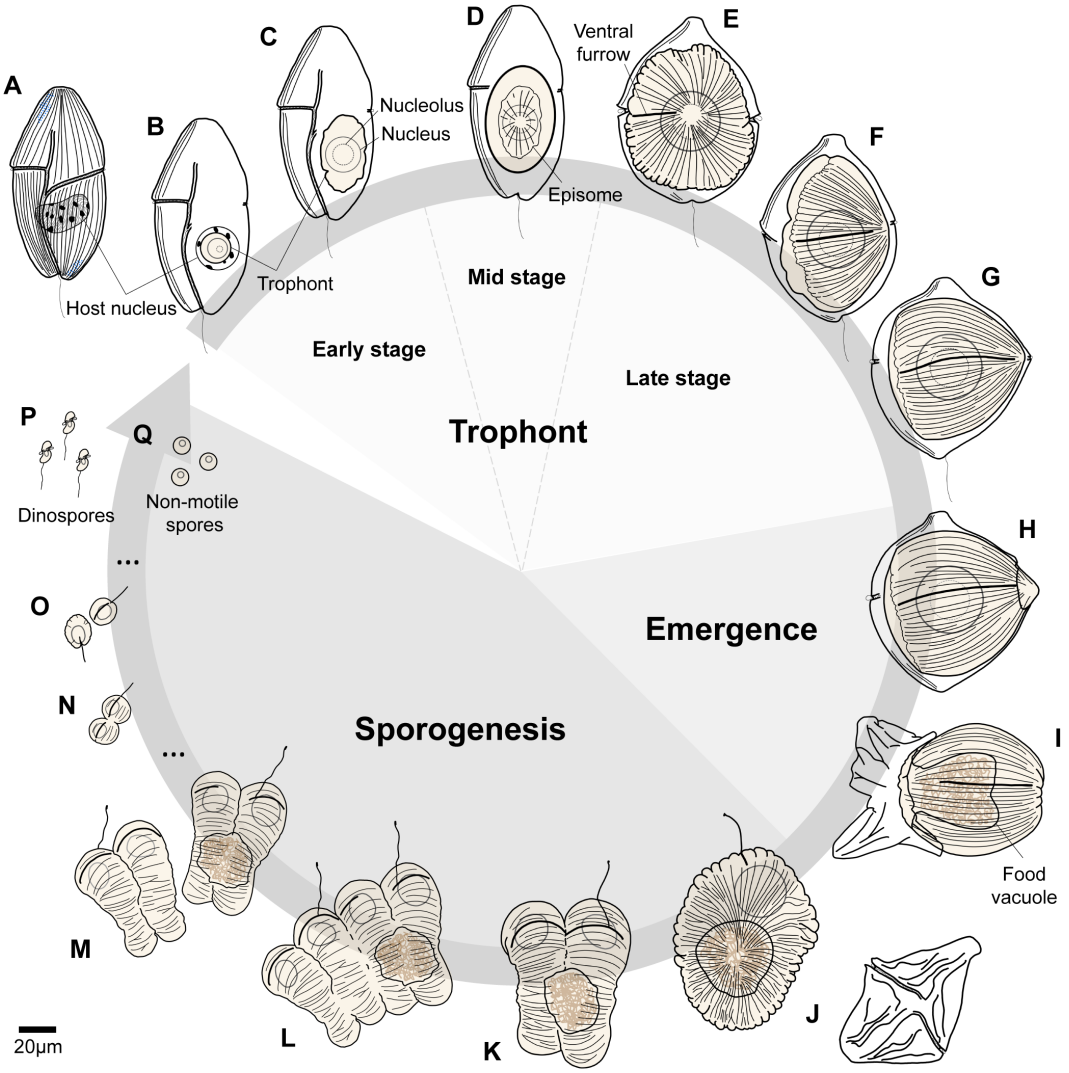

FIGURE 4
Life cycle of *Hobagella saltata* n. gen., n. sp. **(A)** Uninfected host, *Cucumeridinium coeruleum*. **(B, C)** Early stages in the infection cycle before the development of episomal grooves. **(D)** Parasite trophont with a centripetal groove in disc-shaped episome defining mid-stage infections. **(E–G)** Late-stages in the infection cycle during which the parasite trophont becomes acorn-shaped. **(H, I)** Initiation and finalization of parasite egress. **(J)** Recently formed tomont with discarded host pellicle depicted between **(I, J)**. **(K–M)** Sequential steps in the completion of the first sporogenic division, with the initiation of the second division producing a chain of four nascent sporocytes. **(N)** Nascent seventh generation sporocytes. **(O)** Flagellated sporocytes from the ninth division. **(P)** Dinospores and **(Q)** non-motile spherical spores produced at the end of sporogenesis. The arrow indicating life cycle remains open, as we did not observe infection of host cells by spores.

incorporated the host cytoplasm into a food vacuole formed by invagination of the hyposome and constriction of the episomal margin (Figures 4I, 6B). The fully emerged parasite (= tomont) had an elliptical form measuring 82 by 66 µm, was pale yellow in color, and had an acentric food vacuole containing brown host material (Figures 4J, 6C, D). The discarded host pellicle was thin, had a pink-brown color, and appeared empty of cytoplasm. The tomont had 45 bipolar grooves (approximately 10 more than when it was isolated), and a single, 10 µm-long flagellum extending from the ventral furrow. Periodic pulsing of the flagellum produced quick, jerky movements as if the tomont were dancing. In addition to the presence of a flagellum, the ventral furrow differed from the other bipolar grooves by being noticeably wider and deeper.

3.3.4 Sporogenesis

Sporogenesis began almost immediately after parasite egress, with the division plane running perpendicular to the episomal ribs. Nuclear division progressed more quickly than cytoplasmic division and each nascent daughter cell from the division of the tomont (= primary sporocyte) contained a nucleus (Figures 4K, 6E). The posterior daughter cell was slightly larger than the anterior daughter cell and received the flagellum of the tomont as well as a partially digested food vacuole. Cytokinesis of the first division failed to complete prior to the initiation of the second transverse fission, resulting in a short chain of four nascent sporocytes, each having a nucleus (Figures 4L, 6F). The size of the nascent sporocytes forming the chain increased from the anterior to the posterior, with

TABLE 2 Morphometric data for uninfected and infected *Cucumeridinium coeruleum*.

	Mean	SE	Range	n
Uninfected Cucumeridinium coeruleum				
Length (*in vivo*)	105.2	3.21	83.0-125.2	11
Width (*in vivo*)	54.1	3.26	30.5-68.1	11
Nuclear length (*in vivo*)	31.6	3.54	20.9-50.9	7
Nuclear width (*in vivo*)	25.0	2.14	20.3-34.4	6
Length (Protargol-impregnated)	104.4	1.79	73.0-135.6	73
Width (Protargol-impregnated)	62.3	1.41	33.9-85.0	73
Nuclear length (Protargol-impregnated)	22.3	0.51	4.6-31.1	73
Nuclear width (Protargol-impregnated)	15.6	0.26	8.1-19.6	73
Infected Cucumeridinium coeruleum				
Length (*in vivo*)	137.2	5.06	107.7-153.9	9
Width (*in vivo*)	78.8	5.85	63.4-113.4	8
Ventral-dorsal dimension (*in vivo*)	75.2	7.45	67.7-82.6	2
Length (Protargol-impregnated)	129.2	4.15	91.8-150.8	15
Width (Protargol-impregnated)	75.4	2.74	54.2-93.9	15
Nuclear length (Protargol-impregnated)	30.5	3.20	23.3-45.9	11
Nuclear width (Protargol-impregnated)	27.0	3.20	16.7-41.3	11

the posterior-most possessing the parental flagellum and food vacuole. A second flagellum emerged from the second sporocyte in the short chain (counting from anterior to posterior), representing the posterior portion of the anterior daughter cell from the first sporogenic division. Approximately 18 min after the initiation of sporogenesis, the chain of four sporocytes separated due to the completion of cytokinesis associated with the first division. The resulting secondary sporocytes comprised a pair of nascent tertiary sporocytes (Figures 4M, 6G). Sporocyte movement was similar to that of the tomont, and the progress of the next three divisions was as described above, with each division requiring 10–20 min. The sporocyte receiving the degraded food vacuoles eventually failed to undergo additional division. From the sixth division onward, sporocytes were separated prior to the initiation of the next division. Cytokinesis continued to be transverse, and each cell division required 10–15 min (Figures 4N, O, 6H, I). The number of episomal grooves decreased with each division, and the ventral furrow remained noticeably wider and deeper than the other grooves (Figures 6H, I). By the eighth division (Figures 6J, K), the nascent sporocytes possessed only one groove, the ventral furrow, a relatively large nucleus, and a flagellum extending from the presumptive posterior daughter cell. Nine sporogenic divisions resulted in slightly fewer than 512 daughter cells, as the sporocyte containing the spent food vacuole was ultimately unable to complete all divisions. Following the final division, all sporocytes appeared to have a single flagellum. Flagella of sporocytes were 10–15 µm long.

3.3.5 Spores

The ovoid to spherical mono-flagellated cells resulting from sporogenesis transformed into either spherical non-motile spores or motile dinospores (Figures 4P, Q, 6L, M). Non-motile spores had a diameter of 12.1 ± 0.2 µm (n = 9) *in vivo* and lacked a flagellum, while biflagellated dinospores were 11.5 ± 0.4 by 6.0 ± 0.3 µm (n = 24) *in vivo* and 11.2 ± 0.1 by 4.8 ± 0.1 µm (n = 7) after Lugol-fixation. Dinospores had a posterior trailing flagellum and a transverse flagellum wrapped loosely around the cell, with the flagella being 20–25 µm long. (Figures 4P, 6M, Table 3). Following sporogenesis in each parasite, only one type of spore was produced. Five specimens completed sporogenesis, producing dinospores, while one specimen formed spherical non-motile spores. The dinospores remained viable for approximately 3 d after formation, whereas the oval spores remained viable for approximately 4 d.

4 Discussion

4.1 Taxonomic summary

Phylum Miozoa Cavalier-Smith, 1987

Subphylum Myzozoa Cavalier-Smith, 2004 (in Cavalier-Smith and Chao, 2004)

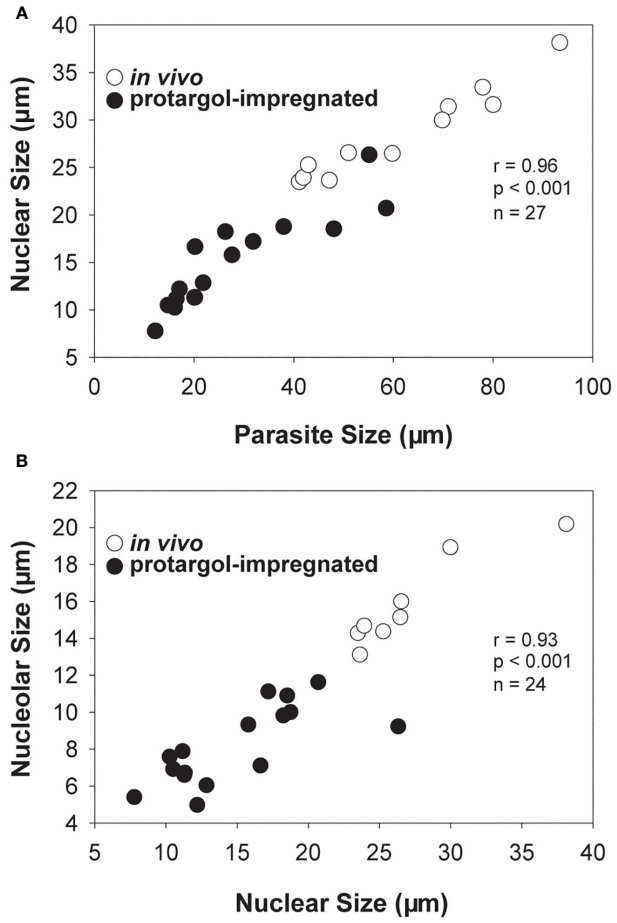

FIGURE 5
Scatter plots and correlation analyses for *Hobagella saltata* morphological data pooled for *in vivo* (open circles) and protargol stained (filled circles) specimens. **(A)** Parasite nuclear size *vs* parasite cell size. **(B)** Parasite nucleolar size *vs* parasite nuclear size. In all cases, "size" was determined as (length + width)/2. Statistical results are for Pearson product-moment correlation.

Superclass Dinoflagellata Bütschli, 1885

Class Syndiniophyceae Loeblich, 1976 (alternatively, Class Syndinea)

Order Ichthyodinida Cavalier-Smith, 2018 (alternatively, Order Ichthyodiniales)

Family Hobagellidae n. fam.

4.1.1 ZooBank LSID

urn:lsid:zoobank.org:act:0D6F4379-3CDB-411C-BB98-4DC6708829D9

4.1.2 Diagnosis

Aplastidic intracellular parasites of marine dinoflagellates. Uninucleate trophont increasing in size without forming food vacuole. Episome covering almost entire trophont at maturity; hyposome highly reduced. Reproduction by palintomy outside host cell, or inside pellicle of moribund host, producing one or more spore types. Dinospores lacking well defined cingulum and sulcus; transverse flagellum wrapping loosely around cell.

4.1.3 Included genera

Hobagella n. gen.

4.1.4 ZooBank LSID

urn:lsid:zoobank.org:act:6A9F7A6E-198A-4368-88D3-35F47F30E42E

4.1.5 Diagnosis

Hobagellidae with disc-shaped episome, centripetal episomal grooves in immature trophont, becoming bipolar with maturation. Fibrous bundles from episome directed toward nucleus, "lamina pharyngae" absent. Tomont motile, with bipolar ribs; ventral furrow bearing one or more flagella. Food vacuole present or absent in tomont; formed via invagination of reduced posterior hyposome. Sporogenesis following rupture of host pellicle or prior to degradation of moribund host pellicle. Sporocytes ribbed, separating after division, or remaining attached as long chain.

4.1.6 Type species

Hobagella saltata n. sp.

4.1.7 Type host

Cucumeridinium coeruleum (Dogiel) Gómez et al., 2015

4.1.8 Etymology

The genus name is derived from Hobag, the Korean word for pumpkin, and the Latin feminine suffix *-ella* indicating a diminutive form of the noun. The vowels of Hobag have the sound of the Latin "ō" and "ā," respectively.

4.1.9 Included species

Hobagella melo n. comb. Cachon, 1964

Hobagella nucleocola n. comb. Cachon, 1964 insertae sedis

Hobagella saltata n. sp.

4.1.10 ZooBank LSID

urn:lsid:zoobank.org:act:4014F161-96E9-4A8F-9255-06F8E64C4F91

4.1.11 Diagnosis

Intranuclear parasite; clear to yellowish trophont, variable in size; 50–110 µm maximum dimension *in vivo* when episomal grooves present. Mature parasite acorn-shaped with near bipolar episomal grooves. Episomal grooves increasing in number with parasite growth; 30–44 in mid- to late-infection; ~45 in tomont. Nucleus and single nucleolus increasing in size with age; nucleolus inconspicuous or absent in mature trophont, tomont, and sporocytes. Food vacuole formed with rupture of host at egress. Sporocytes motile, separating without forming long chain. Two spore types: non-motile spherical spores 11–13 µm diameter *in vivo*; biflagellate, sigmoid dinospores 9–15 µm by 4–9 µm *in vivo*.

4.1.12 Type host

Cucumeridinium coeruleum (Dogiel) Gómez et al., 2015

10.3389/fmars.2023.1296836

TABLE 3 Morphometric data on *Hobagella saltata* n. gen., n. sp.

	Mean	SE	Range	n
Parasite trophonts when isolated (*in vivo*)				
Maximum cell dimension	74.2	4.60	48.6-106.3	15
Minimum cell dimension	54.9	5.16	31.5-80.5	12
Anterior-posterior dimension = cell length	61.3	4.38	45.5-76.0	6
Episome maximum dimension	68.7	5.66	33.7-84.7	8
Episome minimum dimension	57.9	6.05	47.5-75.3	4
Episome anterior-posterior dimension = length	35.4	9.66	9.0-69.4	7
Number of episomal ribs	35.9	1.71	30-44	8
Hyposome anterior-posterior dimension = length	35.8	7.39	22.0-47.3	3
Nuclear length	29.5	1.31	24.1-38.2	11
Nuclear width	27.6	1.59	20.7-38.1	11
Nucleolar length	16.5	0.84	14.3-20.5	8
Nucleolar width	15.1	0.93	11.5-19.9	8
Protargol-impregnated parasite trophonts				
Maximum cell dimension	31.9	4.38	12.9-70.3	17
Minimum cell dimension	26.0	2.98	11.5-53.3	17
Episome maximum axis	53.3	5.11	40.7-70.3	5
Episome minimum axis	45.8	4.92	30.7-57.1	5
Number for episomal ribs	38.5	0.50	38.0-39.0	2
Nuclear length	15.6	1.35	7.9-29.1	16
Nuclear width	14.3	1.09	7.7-23.6	16
Nucleolar length	8.7	0.57	5.4-12.8	16
Nucleolar width	7.7	0.50	4.0-11.3	16
Parasite dinospore				
Length (*in vivo*)	11.5	0.36	8.7-15.0	24
Width (*in vivo*)	6.0	0.27	4.4-9.3	24
Length (Lugol-fixed)	11.2	0.15	10.7-11.7	7
Width (Lugol-fixed)	4.8	0.11	4.5-5.4	7
Parasite oval spore				
Diameter (*in vivo*)	12.1	0.21	11.0-12.7	9

4.1.13 Type habitat

Marine coastal water near Busan, Republic of Korea

4.1.14 Type locality

Yongho Harbor, Republic of Korea (35°08′00″N, 129°06′55″E)

4.1.15 Type material

The name-bearing hapantotype is a slide of protargol-impregnated *Cucumeridinium coeruleum* infected by *Hobagella saltata* and resides at the Nakdonggang National Institute of Biological Resources, Sangju, Republic of Korea (Accession Number NNIBRDN229).

4.1.16 Etymology

The species epithet is the feminine perfect participle of the Latin verb *salto* (= to dance or jump). The name *saltata* refers to the dancing or jumping behavior of pumpkin-shaped tomonts and early sporocytes.

10.3389/fmars.2023.1296836

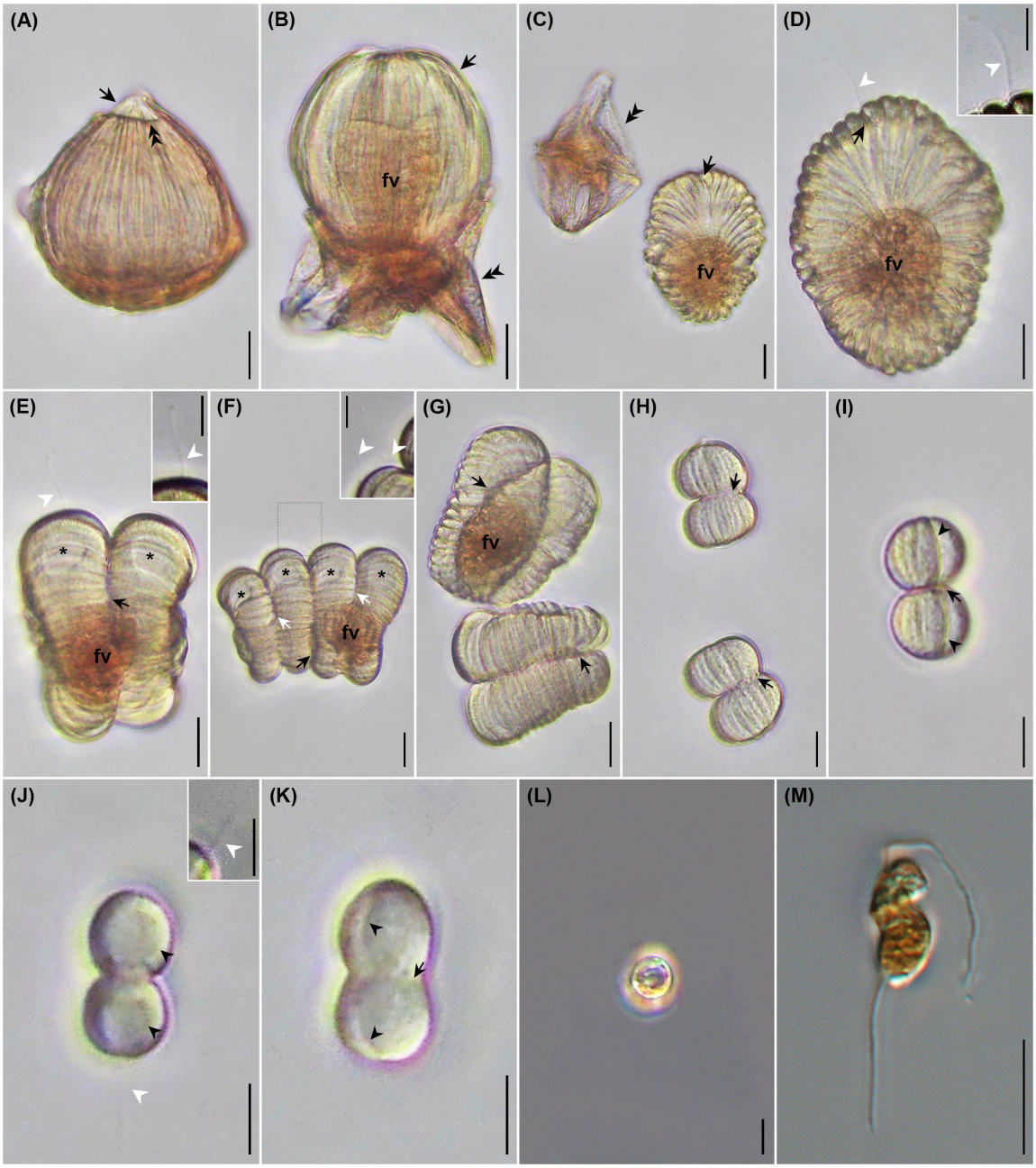

FIGURE 6
Photomicrographs of *Hobagella saltata* n. gen., n. sp. infecting *Cucumeridinium coeruleum in vivo* **(A–L)** and after iodine preservation **(M)**. **(A)** Mature trophont beginning to emerge from the host. Double arrowhead and arrow respectively indicated ruptured host pellicle and parasite apex entering the aqueous medium. **(B)** Emerging parasite (arrow) ingesting host cytoplasm into a food vacuole (fv). Double arrowheads indicate a ruptured host pellicle. **(C)** Recently formed tomont adjacent to empty host pellicle (double arrowheads). Arrow indicates parasite ventral furrow; food vacuole (fv). **(D)** Tomont with flagellum (white arrowhead) extending from ventral furrow (black arrow); food vacuole (fv). Inset: high magnification of tomont flagellum (white arrowhead). **(E)** First sporogenic division showing food vacuole (fv), flagellum (white arrowhead), developing fission furrow (black arrow), and daughter cell nuclei (stars). Inset: high magnification of flagellum (white arrowhead) **(F)** Second sporogenic division showing food vacuole (fv) and daughter cell nuclei (stars). Black and white arrows indicate first and second-division furrows, respectively. Inset: enlargement of area outlined by dots showing flagellum associated with the second nascent sporocyte from the anterior end of the chain; (white arrowheads) located at the first division furrow. **(G)** Daughter cells of first sporogenic division immediately after separation, with each showing a deep division furrow of the second sporogenic division (arrows); food vacuole (fv). **(H)** Daughter cells of the fourth sporogenic division after separation, with each showing a deep division furrow of the fifth sporogenic division (arrows). **(I)** Fifth sporogenic division showing deep division furrow (arrow) and ventral furrow of each daughter cell (arrowheads). **(J)** Eighth sporogenic division showing large nucleus of each daughter (black arrowhead); flagellum (white arrowhead). Inset: high magnification of flagellum from the presumptive posterior daughter cell (white arrowhead). **(K)** Eighth sporogenic division with deep division furrow (arrow) and ventral furrow in each daughter cell (arrowheads). **(L)** Non-motile spherical spores without flagella. **(M)** Dinospore showing bipartite shape and two flagella. Scales bar = 20 µm for **(A–G)** except for inserts. Scale bars for **(H–M)** and inserts = 10 µm.

4.2 Occurrence of *Hobagella* and related parasites infecting dinoflagellates

Hobagella melo parasitizes *Noctiluca scintillans* (= *N. miliaris*), a circumglobally distributed heterotroph that sometimes forms dense blooms (Harrison et al., 2011). *H. melo* was described from Algiers Harbor by Cachon (1964) and was subsequently examined by Hollande (1974) when considering the fast-green staining properties of several dinoflagellates from the Bay of Villefranche sur Mer. Cachon noted that *N. scintillans* was abundant in Algiers Harbor, especially during winter. He also indicated that *H. melo* frequently infected *N. scintillans* in spring and summer but was absent during the season of maximum host abundance because of the inability of the parasites to reproduce at water temperatures during winter (Supplementary Table S1). Given how common *H. melo* was in Cachon's samples, it is surprising that this species has since been reported only once.

Hobagella nucleocola is an uncommon nuclear parasite of *Leptodiscus medusoides*, the latter reported from the western Mediterranean Sea, where it reaches a density of 80 cells/L (Hertwig, 1877; Cachon and Cachon, 1969; Gómez and Furuya, 2005). When describing *H. nucleocola*, Cachon (1964) found approximately 50 specimens in collections from Algier's Harbor in January and May. *H. nucleocola* appears not to have been reported since.

Hobagella saltata, described herein, infects *Cucumeridinium coeruleum*, which, due to its size and striking blue to purple coloration, is a conspicuous heterotrophic species occurring in warm pelagic and coastal environments, including a single report from Korea (Gómez et al., 2015; Shin, 2016; Carnicer et al., 2019). After finding *H. saltata* in 2019, we monitored the occurrence of its host *C. coeruleum* at our primary study area, Yongho Harbor, at weekly intervals from August 2019 to December 2022. These samples revealed the presence of *C. coeruleum* on 10 dates: four days in August 2019; one day in September 2022, and five days in September-October 2022. Thus, *C. coeruleum* is more prevalent in Korean coastal waters than previously recognized but is not a regular member of the coastal microplankton community.

H. saltata appeared to be less common than either *H. melo* or *H. nucleocola*, with only 10 specimens observed *in vivo* for samples obtained in August 2019 and September 2022. While only a few *H. saltata* were observed *in vivo*, our estimates of parasite prevalence based on examination of protargol-stained preparations (2.5–6.3%), indicate that *H. saltata* can, at least in enriched coastal settings, reach moderate infection levels.

Six other syndiniophycean parasites related to *Hobagella saltata* have been reported in the literature but have not been formally described (Supplementary Table S1). Cachon (1964) studied a species (likely representing more than one species) of *Euduboscquella* infecting various dinoflagellate hosts in Algiers Harbor, including thecate, athecate, phototrophic, and heterotrophic species. Yoo et al. (2022) provided images and rRNA gene sequences for three parasites from Yongho Harbor (other than the one we report here as *H. saltata*), referring to them as *Euduboscquella* sp. ex *Gyrodinium* sp. (OP445722-23), *Euduboscquella* sp. ex *Gyrodinium* cf. *ochraceum* (OP445724), and *Euduboscquella* sp. ex *Gyrodinium* sp. (OP445725). Lastly, Holt et al. (2023) provided images, single-cell transcriptomic data and rRNA gene sequences for three unidentified Ichthyodinida parasites from Heriot Bay, Canada, and Piscadera Bay, Curaçao. Two of the parasites, Ichthyodinida sp. (OR427349) and Ichthyodinida sp. (OR427354), infect the dinoflagellates *Warowia* sp. and *Polykrikos* sp., respectively, while Ichthyodinida sp. (OR427350) has an unspecified host and is excluded from the discussion of this study.

None of these parasites were very common, as Cachon (1964) only observed three parasites per 1000 host cells (0.3% prevalence), while Yoo et al. (2022) found only two specimens of *Euduboscquella* sp. ex *Gyrodinium* sp. (OP445722-23) and one specimen each of *Euduboscquella* sp. ex *Gyrodinium* cf. *ochraceum* (OP445724) and *Euduboscquella* sp. ex *Gyrodinium* sp. (OP445725). Hereafter, we refer to *Euduboscquella* sp. (OP445722-23) and *Euduboscquella* sp. (OP445724) as *Hobagella*-like species.

4.3 Potential effects of typhoons on the occurrence of *H. saltata* in Yongho and Youngdo Harbors

Typhoons alter ecosystems in ways that can influence the abundance and distribution of organisms. For example, typhoons promote vertical mixing of the water column causing decreased sea surface temperature (SST), increased nutrient concentrations in surface water, upward distribution of stratified populations (e.g., deep chlorophyll maxima as occur in the East Sea and Korea Strait), and subsequently enhanced phytoplankton biomass (Son et al., 2006; Kim et al., 2012; Rho et al., 2012; Shang et al., 2015; Chang et al., 2017; Ma et al., 2021; Son et al., 2022). They can also amplify or generate nutrient-rich, cold-core eddies that promote phytoplankton blooms and can potentially move planktonic populations landward (Llinás et al., 2009; Lee et al., 2020; Ma et al., 2021). Finally, storm-related events associated with typhoons (e.g., nutrient enrichment due to mixing or local heavy rainfall) can result in increased phytoplankton biomass and shifts in community composition (Baek et al., 2020).

Since both occasions when we encountered *H. saltata* followed a typhoon, it seems plausible that the occurrence of infected *C. coeruleum* in our study area may have been influenced by storm related processes. As shown in Figure 2, surface water temperature in our study area increased to ~27°C in 2019 and to ~25°C in 2022, a few days prior to Typhoon KROSA and Typhoon HINNAMNOR reaching 35°N (the latitude of Busan, ROK) on 15 August 2019 and 5 September 2022, respectively. The day after each storm moved past 35°N, the water temperature in our study area began to decrease, with *H. saltata* detected 10–12 d later in 2019 and 4 d later in 2022. Similarly, SST contour plots for the East Sea (Sea of Japan) in August 2019 and September 2022 (open source data available at Streamlit v1.12.2, https://ocean-temperature-monitoring-bryanrvallejo.streamlit.app/) showed increasing water temperature in the Korea Strait as typhoons KROSA and HINNAMNOR moved northward, followed by decreasing water temperatures after the typhoons passed north of 35°N. The increase

in SST in the Korea Strait and near the Korean coast appeared to be associated with the increased intensity of the East Korea Warm Current (EKWC) and the Tsushima Warm Current (TWC) preceding and during the storms. For example, SST near the southeastern coast of Korea one to two weeks prior to Typhoon KROSA ranged from 18–24°C (Figures 7A, B), possibly reflecting the upwelling of cool water, as frequently occurs in that region during summer (Yoo and Park, 2009; Kim et al., 2023), while offshore water extending to the eastern side of the Korea Strait was 25–27°C. When Typhoon KROSA was positioned south of Japan (24-26°N) on 12 August, the lens of cool water adjacent to the Korean coast was replaced by water ranging from 24–26°C (Figure 7C), with temperature rising to 27–28°C by 15 August as the storm reached 35°N, crossing Japan to the East Sea (Figure 7D). At that time, a well-defined footprint of elevated water temperature (29–30°C) branched around Tsushima Island indicating strengthening of the TWC and EKWC. Two days later (Figure 7E), water near the southeastern Korean coast appeared to cool (23–26°C), and a lens of cooler water consistent with upwelling was evident on 23 and 26 August when *C. coeruleum* and *H. saltata* were respectively first detected (Figures 7F, G). The host and parasite were no longer detectable on 29 August as the SST contours began to reflect the pre-storm conditions (Figure 7H).

Given that *C. coeruleum* was not found in samples collected on 8–14 August, before Typoon KROSA reached 35°N on 15 August, or in samples from 19, 21, and 22 August as a lens of cool water indicative of upwelling reappeared on the southeastern coast of Korea (Yoo personal observations), it seems unlikely that a population of *C. coeruleum* having appreciable abundance was advected to our study area in northward-flowing warm surface water. It is, however, conceivable that a population of *C. coeruleum*, of sufficiently low abundance to be detected in the net sample, was transported to our study area and subsequently increased in population size. In this scenario, *H. saltata* could have been present at a low prevalence in the advected *C. coeruleum* population, persisted at a low prevalence as host densities increased, and then became more prevalent as the host population reached threshold densities to promote more rapid transmission of the parasite. Alternatively, *H. saltata* might not have been present in the advected *C. coeruleum* population, but rather in some other host species in our study area, with transmission to *C. coeruleum* occurring after advection and reproduction in our study area. While either of these two related scenarios could explain our observations, we tend to reject them for two reasons: (1) both scenarios encompass an increase in host abundance and parasite prevalence over time, whereas our observations show a decline in the prevalence of *H. saltata* from 5–6% on 26–27 August to 2.5% on August 28, with the absence of *C. coeruleum* afterward; (2) we believe it unlikely that we would have failed to observe *C. coeruleum*, even if in low abundance, when examining net samples collected on multiple dates between 8–22 August as discussed above. Thus, we favor a third hypothesis involving the transport of a subsurface population of *C. coeruleum* infected by *H. saltata* beneath warm surface water moving northward as Typhoon KROSA crossed Japan and entered the East Sea. Not only might *C. coeruleum* persist at depth in association with the deep chlorophyll maxima known to occur in the East Sea and Korea Strait during summer (Kim et al., 2012; Rho et al., 2012), but infection by *H. saltata* might cause *C. coeruleum* to concentrate at depth, just as infection of the dinoflagellate *Akashiwo sanguinea* by another syndiniophycean parasite, *Amoebophrya* cf. *ceratii*, induces positive geotaxis and negative phototaxis of host cells, resulting in the accumulation of infected hosts at the density discontinuity (Park et al., 2002). In the third scenario, the detection of hosts and parasites would not require the growth of the *C. coeruleum* population after advection into the study area. Furthermore, the short period (3 d) during which we were able to find host and parasite is not surprising given that continued upwelling without continuous introduction of additional infected host cells would soon dilute or export the introduced population of *C. coeruleum* infected by *H. saltata*. If supported by future research, the hypothesis outlined above would reveal previously unrecognized mechanisms for distributing cryptic parasites of planktonic dinoflagellates that may alter organism biogeography under ongoing global change in SST.

4.4 Morphological comparison of *Hobagella* species, *Euduboscquella* species, and related parasites infecting dinoflagellates

Shield structure, sporogenetic pattern, and spore morphology are considered important morphological features in differentiating *Euduboscquella* species that infect tintinnid ciliates (Coats and Bachvaroff, 2013; Choi et al., 2021). In addition to those characters, Yoo et al. (2022) found that the shape and color of trophonts near maturity are useful in distinguishing MALV Group I parasites that infect dinoflagellates. Here, we add expansion of the episome to produce near bipolar grooves and the presence of fibrous bundles derived from the episome and extending to the nucleus as valuable characters in sorting these related parasites. The constellation of characters defined above provides useful genus and species boundaries for *Euduboscquella, Hobagella*, and *Hobagella*-like species and may elucidate morphological evolutionary patterns among these parasites (Supplementary Table S1).

Three of the undescribed species, *Euduboscquella* sp. (Cachon, 1964), *Euduboscquella* sp. ex *Gyrodinium* sp. (OP445725; Yoo et al., 2022), and Ichthyodinida sp. (OR427349; Holt et al., 2023) considered in Supplementary Table S1 can be easily separated from *Hobagella* and *Hobagella*-like species by the former's non-centripetal arrangement of their episomal grooves (i.e., brain-like pattern or apparent alignment in rows). In addition, *Euduboscquella* sp. described by Cachon (1964) seems to have a rudimentary "lamina pharyngae," whereas *Hobagella* species lack a "lamina pharyngae." The three described species of *Hobagella* share the following characteristics: centripetal episomal grooves, the presence of fibrous bundles derived from the episome and directed toward the nucleus, nearly bipolar episomal grooves during late-infection, parasite egress via rupture of the host pellicle (either due to pressure exerted by the parasite or through degradation of the moribund host), and persistence of bipolar grooves in the tomont and

sporocytes. All of these traits, except for the presence of centripetal episomal grooves, are absent in *Euduboscquella* species and thus represent genus-level characters. The two species of *Euduboscquella* that have centripetal episomal grooves (*E. cnemata* and *E. costata*) fail to retain grooves in the extracellular life history stages.

H. saltata differs from *H. melo* in terms of trophont size, color during late-infection, the shape of the mature trophont, sporogenesis in the external environment rather than inside the moribund host, and the presence of a food vacuole in the tomont. *H. saltata* diverges from *H. nucleocola* by the coloration of the maturing trophont, number of episomal grooves, shape of the mature trophont, and pattern of sporogenesis. *H. saltata* resembles *Hobagella*-like sp. ex *Gyrodinium* sp. (OP445722-23), differing only in trophont size and sporogenic pattern, although the number of episomal grooves is unknown in the latter. Additionally, it contrasts with *Hobagella*-like sp. ex *Gyrodinium* cf. *ochraceum* (OP445724) in terms of trophont color, trophont shape at maturity, and number of episomal grooves. Lastly, Ichthyodinida sp. (OR427354) reported by Holt et al. (2023) is difficult to compare due to lack of information on morphological and developmental features, but it is similar to *H. saltata* in trophont size and groove pattern. While it is tempting, based on morphological features, to consider *Hobagella*-like species (OP445722-24) and unidentified Ichthyodinida sp. (OR427354) as congeners of *H. saltata*, molecular data discussed below advise caution.

4.5 Implications of rRNA gene phylogeny in the classification of MALV group I parasites

Phylogenetic relationships among *Euduboscquella*, *Hobagella*, *Hobagella*-like species and three unidentified species of Ichthyodinida recently reported by Holt et al. (2023) were inferred from MALV Group I phylogeny based on SSU rRNA gene sequences (Figure 8). *Euduboscquella* species infecting tintinnids form their own specific subclade within clade 4 of the MALV Group I phylogeny as noted in previous reports (Bachvaroff et al., 2012; Yoo et al., 2022; Holt et al., 2023). One of the four parasites of dinoflagellates reported by Yoo et al. (2022), *Euduboscquella* sp. ex *Gyrodinium* sp.(OP445725) and the unidentified Ichthyodinida sp. (OR427349) reported by Holt et al. (2023), exhibited traits consistent with those of the genus *Euduboscquella*. Although *Euduboscquella* sp. ex *Gyrodinium* sp. (OP445725) and Ichthyodinida sp. (OR427349) were placed in clade 4 of the MALV Group I phylogeny (Figure 8)), they did not belong to the *Euduboscquella* clade proposed by Bachvaroff et al. (2012). Thus, a more comprehensive examination of the morphology and development of *Euduboscquella* sp. (OP445725) and Ichthyodinida sp. (OR427349) is necessary to assess whether they belong to the genus *Euduboscquella* or to a new genus.

Hobagella saltata, *Hobagella*-like sp. (OP445724), and Ichthyodinida sp. (OR427354) in Supplementary Table S1 branched within clade 3 of the MALV Group I. Thus, given the morphological and developmental similarities among the three species, *Hobagella*-like sp. (OP445724) and Ichthyodinida sp. (OR427354) are likely congeners of *H. saltata*. The final novel species *Hobagella*-like sp. ex *Gyrodinium* sp. (OP445722-23) in Supplementary Table S1, is morphologically very similar to *H. saltata* but differs developmentally by producing a long chain of sporocytes, rather than generating multiple separated sporocytes during sporogenesis. In the SSU rRNA phylogeny (Figure 8), *Hobagella*-like sp. (OP445722-23) did not diverge within clade 3 but instead branched in a basal lineage to Group I clades 3, 4, and 6 (encompassing *Ichthyodinium chabelardi* and known

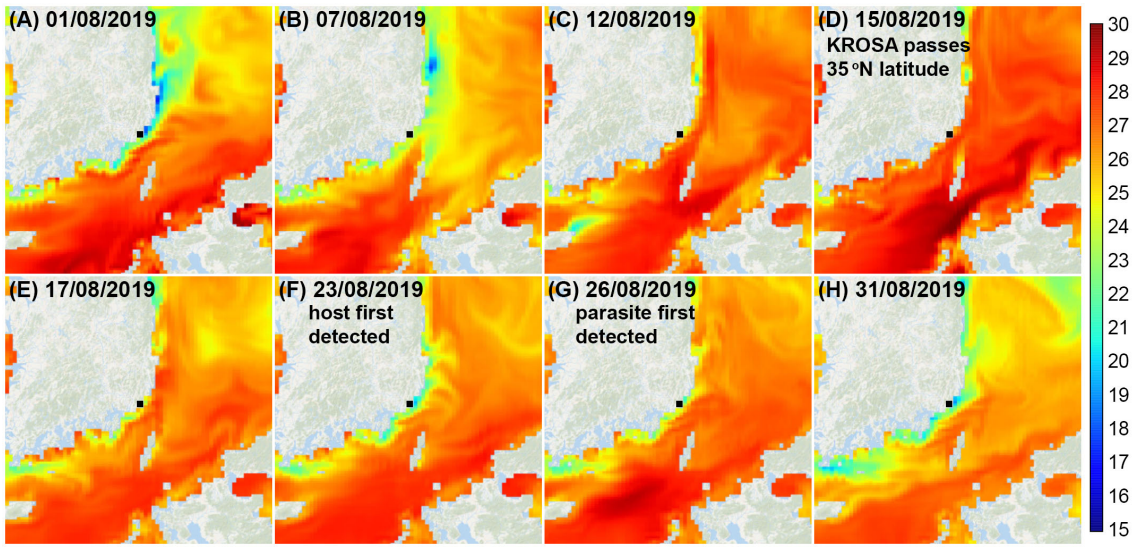

FIGURE 7
Sea surface temperature contours for the East Sea and Korea Strait from 1-31 August 2019 **(A–H)**. Typhoon KROSA was positioned south of Japan (24-26°N) on 12 August and moved northward over Japan and into the East Sea passing 35°N on 15–16 August. *Cucumeridinium coeruleum* was first detected in Yongho Harbor on 23 August, with *Hobagella saltata* first observed on 26 August. Contour plots are open-source data provided by Streamlit v1.12.2: (https://ocean-temperature-monitoring-bryanrvallejo.streamlit.app/).

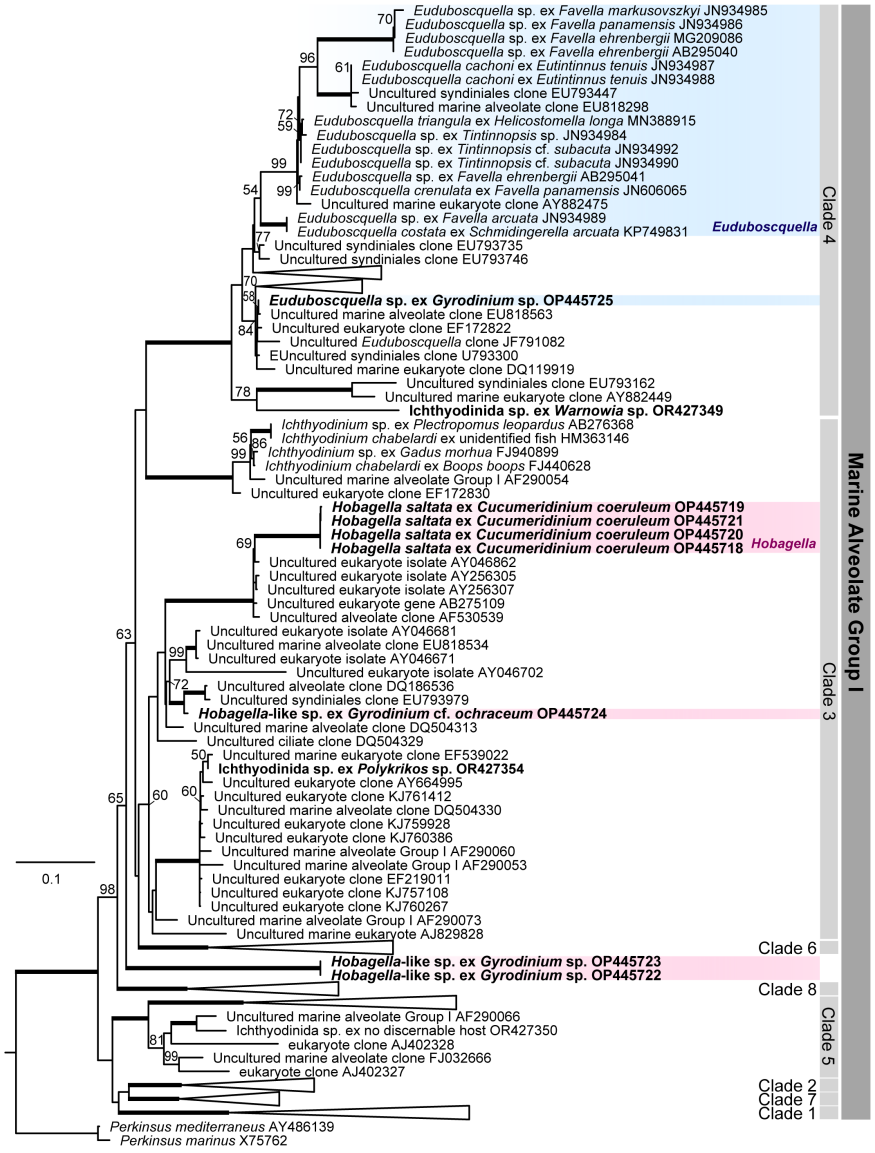

FIGURE 8
Marine Alveolate Group I phylogeny inferred from SSU rRNA gene sequences. Likelihood Bootstrap Support; LBS greater than 50% are shown above nodes. Fully supported branches (100%) are represented by thick lines. Parasites infecting dinoflagellates represent in bold, *Euduboscquella* species in blue box, and *Hobagella* and *Hobagella*-like species in red box.

Euduboscquella species) with moderate support. It is somewhat surprising that *Hobagella* and *Hobagella*-like species, which show different patterns of sporogenesis, diverge in the SSU rRNA phylogeny, given that *Euduboscquella* species that grouped together as a subclade of Group I clade 4 exhibit four different patterns of sporogenesis (Choi et al., 2021). Nonetheless, it is possible that future morphological and molecular studies will require erection of a new genus for *Hobagella*-like sp. (OP445722-23). Given that the pattern of sporogenesis may be an important characteristic in sorting the genera of *Hobagella*-like parasites, we included *Hobagella nucleocola*, for which molecular data are unavailable, provisionally as a congener of *H. saltata* and *H. melo*.

Data availability statement

The datasets analyzed for this study can be found in the NCBI [https://www.ncbi.nlm.nih.gov/genbank/, Accession nos. OP445718–OP445721, OP465226–OP465229, and OP465233].

Author contributions

JY: Formal analysis, Investigation, Writing – original draft, Conceptualization. SK: Conceptualization, Formal analysis, Funding acquisition, Investigation, Writing – review & editing.

DC: Conceptualization, Formal analysis, Investigation, Writing – review & editing.

Funding

The author(s) declare financial support was received for the research, authorship, and/or publication of this article. This research was supported by Korea Institute of Marine Science & Technology (KIMST) funded by the Ministry of Oceans and Fisheries (RS-2023-00256330, Development of risk managing technology tackling ocean and fisheries crisis around Korean Peninsula by Kuroshio Current) and by the National Research Foundation (NRF-2022M316A1085991 and NRF-2020R1F1A1074301).

Acknowledgments

We would like to thank Prof. Jae-Hyoung Park in Pukyong National University for introducing us to the Ocean SST Monitoring website and for his valuable comments.

Conflict of interest

The authors declare that the research was conducted in the absence of any commercial or financial relationships that could be construed as a potential conflict of interest.

Publisher's note

Supplementary material

The Supplementary Material for this article can be found online at: https://www.frontiersin.org/articles/10.3389/fmars.2023.1296836/full#supplementary-material

References

Bachvaroff, T. R., Kim, S., Guillou, L., Delwiche, C. F., and Coats, D. W. (2012). Molecular diversity of the syndinean genus *Euduboscquella* based on single cell PCR analysis. *Appl. Environ. Microbiol.* 78, 334–345. doi: 10.1128/AEM.06678-11

Baek, S. H., Lee, M., Park, B. S. D., and Lim, Y. K. (2020). Variation in phytoplankton community due to an autumn typhoon and winter water turbulence in southern Korean coastal waters. *Sustainability* 12, 2781. doi: 10.3390/su12072781

Bütschli, O. (1885). "Protozoa. Abtheilung II. Mastigophora," in *Klassen und Ordnungen des Thier-Reichs*, vol. 1 . Ed. B. H. G. (Leipzig: C. F. Winter), 611–1097.

Cachon, J. (1964). Contribution a l'étude des péridiniens parasites. cytologie, cycles évolutifs. *Ann. Sci. Nat. Zool.* 6, 1–158.

Cachon, J., and Cachon, M. (1969). Contribution á l'étude des Noctilucidae Saville-Kent. Évolution, morphologique, cytologie, systématique. II. Les Leptodiscinae. *Protistologica* 5, 11–33.

Carnicer, O., de la Fuente, P., Canepa, A., Keith, I., Rebolledo-Monsalve, E., Diogène, J., et al. (2019). Marine dinoflagellate assemblage in the Galápagos Marine Reserve. *Front. Mar. Sci.* 6. doi: 10.3389/fmars.2019.00235

Cavalier-Smith, T. (1987). The origin of eukaryote and archaebacterial cells. *Ann. N.Y. Acad. Sci.* 503, 17–54. doi: 10.1111/j.1749-6632.1987.tb40596.x

Cavalier-Smith, T., and Chao, E. E. (2004). Protalveolate phylogeny and systematics and the origins of Sporozoa and dinoflagellates (phylum Myzozoa nom. nov.). *Eur. J. Prot.* 40, 185–212. doi: 10.1016/j.ejop.2004.01.002

Cavalier-Smith, T. (2018). Kingdom Chromista and its eight phyla: a new synthesis emphasising periplastid protein targeting, cytoskeletal and periplastid evolution, and ancient divergences. *Protoplasma* 255, 297–357. doi: 10.1007/s00709-017-1147-3

Chang, Y.-L., Miyazawa, Y., Oey, L.-Y., Kodaira, T., and Huang, S. (2017). The formation processes of phytoplankton growth and decline in mesoscale eddies in the western North Pacific. *Ocean J. Geophys. Res. Oceans.* 122, 4444–4455. doi: 10.1002/2017JC012722

Chatton, E. (1920). Les Péridiniens parasites: morphologie, reproduction, ethologie. *Arch. Zool. Exp. Gen.* 59, 1–475.

Choi, J. M., Jung, J. H., Kim, K. H., Coats, D. W., and Kim, Y. O. (2021). A novel parasitic, syndinean dinoflagellate *Euduboscquella triangula* infecting the tintinnid *Helicostomella longa*. *Front. Mar. Sci.* 8. doi: 10.3389/fmars.2021.720424

Coats, D. W., and Bachvaroff, T. R. (2013). "Parasites of tintinnids," in *The Biology and Ecology of Tintinnid Ciliates: Models for Marine Plankton*. Eds. J. R. Dolan, D. J. S. Montagnes, S. Agatha, D. W. Coats and G. McManus (Chichester: Wiley-Blackwell), 145–170. doi: 10.1002/9781118358092.ch6

Coats, D. W., Bachvaroff, T. R., and Delwiche, C. F. (2012). Revision of the family Duboscquellidae with description of *Euduboscquella crenulata* n. gen., n. sp. (Dinoflagellata, Syndinea), an intracellular parasite of the ciliate *Favella panamensis* Kofoid & Campbell 1929. *J. Eukaryot. Microbiol.* 59, 1–11. doi: 10.1111/j.1550-7408.2011.00588.x

Coats, D. W., and Heinbokel, J. F. (1982). A study of reproduction and other life-cycle phenomena in planktonic protists using an acridine orange fluorescence technique. *Mar. Biol.* 67, 71–79. doi: 10.1007/BF00397096

Coats, D. W., and Moon, E. (2022). Ultrastructure of selected life history stages of the parasitic dinoflagellate *Euduboscquella cachoni*. *J. Eukaryot. Microbiol.* 69, e12921. doi: 10.1111/jeu.12921

Corliss, J. O. (1984). The Kingdom Protista and its 45 phyla. *BioSystems* 17 (2), 87–126. doi: 10.1016/0303-2647(84)90003-0

Fensome, R. A., Taylor, F. J. R., Norris, G., Sarjeant, W. A. S., Wharton, D. I., and Williams, G. L. (1993). *A Classification of Living and Fossil Dinoflagellates* (Hanover, PA: Micropaleontology Special Publication 7, 1–245. Sheridan Press), 351. p.

Gómez, F., and Furuya, K. (2005). Leptodiscaceans (Noctilucales, Dinophyceae) from the Pacific Ocean: First records of *Petalodinium* and *Leptodiscus* beyond the Mediterranean Sea. *Eur. J. Protistol.* 41, 231–239. doi: 10.1016/j.ejop.2005.05.003

Gómez, F., López-García, P., Takayama, H., and Moreira, D. (2015). *BaleChina* and the new genus *Cucumeridinium* gen. nov. (Dinophyceae), unarmored dinoflagellates with thick cell coverings. *J. Phycol.* 51, 1088–1105. doi: 10.1111/jpy.12346

Harrison, P. J., Furuya, K., Glibert, P. M., Xu, J., Liu, H. B., Yin, K., et al. (2011). Geographical distribution of red and green *Noctiluca scintillans*. *Chin. J. Oceanol. Limn.* 29 (4), 807–831. doi: 10.1007/s00343-011-0510-z

Hertwig, R. (1877). Ueber *Leptodiscus medusoides*, eine neue den Noctiluciden verwandte Flagellate. *Jenaische Z. Naturwiss. NF* 11, 307–323.

Hollande, A. (1974). Étude comparée de la mitose syndinienne et de celle des péridiniens libres et des hypermastigines infrastructure et cycle évolutif des syndinides parasites de radiolaires. *Protistologica* 10, 413–451.

Holt, C. C., Hehenberger, E., Tikhonenkov, D. V., Jacko-Reynolds, V. K., Okamoto, N., Cooney, E. C., et al. (2023). Multiple parallel origins of parasitic Marine Alveolates. *Nat. Commun.* 14 (1), 7049. doi: 10.1038/s41467-023-42807-0

Katoh, K., Rozewicki, J., and Yamada, K. D. (2019). MAFFT online service: multiple sequence alignment, interactive sequence choice and visualization. *Briefings Bioinf.* 20 (4), 1160–1166. doi: 10.1093/bib/bbx108

Kim, D., Choi, J.-G., Park, J., Kwon, J.-I., Kim, M.-H., and Jo, Y.-H. (2023). Upwelling processes driven by contributions from wind and current in the Southwest East Sea (Japan Sea). *Front. Mar. Sci.* 10. doi: 10.3389/fmars.2023.1165366

Kim, D., Yang, E. J., Kim, K. H., Shin, C.-W., Park, J., Yoo, S., et al. (2012). Impact of an anticyclonic eddy on the summer nutrient and chlorophyll a distributions in the Ulleung Basin, East Sea (Japan Sea). *ICES J. Mar. Sci.* 69 (1), 23–29. doi: 10.1093/icesjms/fsr178

Kumar, S., Stecher, G., Li, M., Knyaz, C., and Tamura, K. (2018). MEGA X: Molecular evolutionary genetics analysis across comput- ing platforms. *Mol. Biol. Evol.* 35, 1547–1549. doi: 10.1093/molbe v/msy096

Lee, J.-H., Moon, J.-H., and Kim, T. (2020). Typhoon-triggered phytoplankton bloom and associated upper-ocean conditions in the northwestern Pacific: Evidence from satellite remote sensing, Argo Profile, and an Ocean Circulation Model. *J. Mar. Sci. Eng.* 8, 788. doi: 10.3390/jmse8100788

Llinás, L., Pickart, R. S., Mathis, J. T., and Smith, S. L. (2009). Zooplankton inside an Arctic Ocean cold-core eddy: Probable origin and fate. *Deep-Sea Res. II.* 56, 1290–1304. doi: 10.1016/j.dsr2.2008.10.020

Loeblich, A. R. III. (1976). Dinoflagellate evolution: speculations and evidence. *J. Protozool.* 23 (1), 13–28. doi: 10.1111/j.1550-7408.1976.tb05241.x

Lohmann, H. (1908). Untersuchungen zur feststellung des vollständigen gehaltes des meeres an plankton. *Wiss. Meeresunters. Kiel.* 10, 129–307.

Ma, C., Zhaoa, J., Ai, B., Suna, S., Zhang, G., Huang,, et al. (2021). Assessing responses of phytoplankton to consecutive typhoons by combining Argo, remote sensing and numerical simulation data. *Sci. Total Environ.* 790, 148086. doi: 10.1016/j.scitotenv.2021.148086

Montagnes, D. J. S., and Lynn, D. H. (1993). "A quantitative protargol stain (QPS) for ciliates and other protists," in *Handbook of Methods in Aquatic Microbial Ecology*. Eds. P. F. Kemp, B. F. Sherr, E. B. Sherr and J. J. Cole (Boca Raton: Lewis Publishers), 229–240. doi: 10.1201/9780203752746-28

Park, M. G., Cooney, S. K., Kim, J. S., and Coats, D. W. (2002). Effects of parasitism on diel vertical migration, phototaxis/geotaxis, and swimming speed of the bloom-forming dinoflagellate *Akashiwo sanGuinea*. *Aquat. Microb. Ecol.* 29, 11–18. doi: 10.3354/ame029011

Rho, T., Lee, T., Kim, G., Chang, K.-I., Na, T., and Kim, K.-R. (2012). Prevailing subsurface chlorophyll maximum (SCM) layer in the East Sea and its relation to the physico-chemical properties of water masses. *Ocean Polar Res.* 34 (4), 413–430. doi: 10.4217/OPR.2012.34.4.413

Shang, X., Zhu, H., Chen, G., Xu, C., and Yang, Q. (2015). Research on cold core eddy change and phytoplankton bloom induced by typhoons: Case studies in the South China Sea. *Adv. Meteorol.* 2015, 1–19. doi: 10.1155/2015/340432

Shin, E. Y. (2016). "Dinoflagellates," in *Protists of Korea*, vol. 1 . Ed. J. K. Choi (Incheon: The Korean Society of Protistologists and Academy Information Center), 71–526. Available at: https://product.kyobobook.co.kr/detail/S000001543492.

Son, J.-H., Heo, K.-Y., Choi, J.-W., and Kwon, J. (2022). Long–lasting upper ocean temperature responses induced by intense typhoons in mid–latitude. *Sci. Rep.* 12, 5752. doi: 10.1038/s41598-022-09833-2

Son, S. H., Platt, T., Bouman, H., Lee, D. K., and Sathyendranath, S. (2006). Satellite observation of chlorophyll and nutrients increase induced by Typhoon Megi in the Japan/East Sea. *Geophysical Res Lett.* 33, L05607. doi: 10.1029/2005GL025065

Yoo, J., Coats, D. W., and Kim, S. (2022). Syndinian dinoflagellates of the genus *Eudubosquella* are paraphyletic. *J. Eukaryot. Microbiol.* 70, e12953. doi: 10.1111/jeu.12953

Yoo, S., and Park, J. (2009). Why is the southwest the most productive region of the East Sea/Sea of Japan? *J. Mar. Syst.* 78, 301–315. doi: 10.1016/j.jmarsys.2009.02.014